A Single Metal Ion Plays Structural and Chemical Roles in an Aminoacyl-Transferase Ribozyme†

Amber Flynn-Charlebois, Nick Lee, and Hiroaki Suga*

Department of Chemistry, 657 Natural Sciences Complex, University at Buffalo, State University of New York, Buffalo, New York 14260-3000

Received May 30, 2001; Revised Manuscript Received July 27, 2001

ABSTRACT: Catalytically active RNA molecules rely on metal ions for structural and/or catalytic functions. Our in vitro selected aminoacyl-transferase ribozyme is no exception, as it employs a single fully hydrated Mg^{2+} ion for catalysis [Suga, H., et al. (1998) *Biochemistry 37*, 10118−10125]. Here we report the essential catalytic residues of the ribozyme and their spatial arrangement in the relation to the metal binding site. Evidence obtained using a combination of Pb^{2+} and Tb^{3+} hydrolytic cleavage assays on wild type and mutant ribozymes revealed a cooperative metal binding site that consists of the tandem G:U wobble pairs in P1 and consecutive G:U and U:A pairs in P3. The formation of this concerted Mg^{2+} binding site positions the P1 and P3 helices in a parallel manner, placing the L3 tetraloop in close proximity to the internal guide sequence (IGS, substrate binding site), which is adjacent to P1. Certain monovalent metal ions inhibit catalysis at low concentrations but support catalysis at high concentrations. These analyses imply that the Mg^{2+} ion plays both structural and chemical roles and that it brings about the significant rate acceleration in aminoacyl-transfer in concert with the L3-IGS long-range interaction.

The discovery of self-splicing and nuclease ribozymes introduced the notion that RNA molecules could possess catalytic functions similar to protein enzymes (*1*−*3*). Although naturally occurring ribozymes found to date catalyze only phosphodiester bond transfer, recent examples of novel ribozymes isolated by in vitro evolution show more versatile catalytic functions (*4*−*6*). Aminoacyl-transferase ribozyme (ATRib)[1] is an in vitro evolved ribozyme that catalyzes aminoacyl transfer from a donor hexanucleotide to an acceptor tRNA via a covalent aminoacyl-ribozyme intermediate (*7*, *8*). We have recently reported that a ribozyme, evolved from an RNA pool consisting of ATRib-random sequences, is able to execute specific amino acid recognition and charging of tRNA (*9*). Therefore, this ribozyme exhibits two of the essential functions of the contemporary protein enzyme, aminoacyl-tRNA synthetase (*10*).

Earlier work has shown that the 82-nt ATRib arranges itself into a cloverleaf secondary structure that consists of four stems and three loops referred to as P1−P4 and L2−L4, respectively, and the internal guide sequence (IGS) that is responsible for binding the hexanucleotide substrate (Figure 1A) (*8*). A simple template ribozyme, in which the entire P2−P4 domain was replaced with a stable tetraloop (Figure 1B), exhibited 3 orders of magnitude lower activity than ATRib, implying the necessity of the P2−P4 domain for efficient catalysis (*8*). ATRib is a metalloenzyme that requires a single catalytic Mg^{2+} ion in the fully hydrated form. Evidence for the role of this catalytic metal ion was obtained by using $Co(NH_3)_6^{3+}$ as a substitute for $Mg(H_2O)_6^{2+}$ (*11*). When the tandem G:U wobble base pairs near the acylation site were mutated to tandem G:C pairs, a 50-fold reduction in activity was observed (*7*, *8*, *11*), indicating the necessity of these tandem G:U wobble base pairs for catalytic

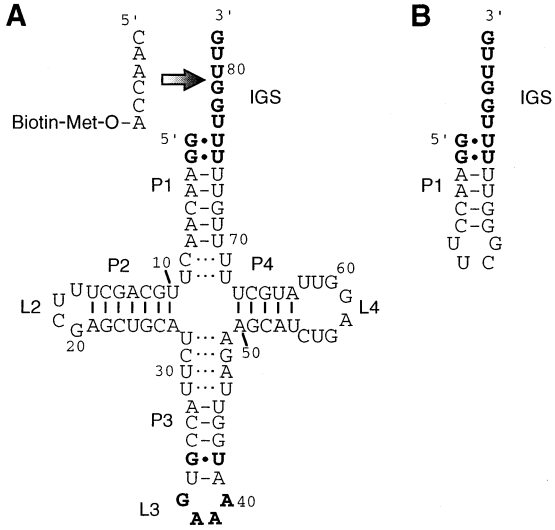

FIGURE 1: Secondary structure of acyl-transferase ribozyme (ATRib). (A) The 82-nt wild-type ATRib and its substrate. Bold letters denote critical bases for activity determined in this study. (B) Secondary structure of a 22-nt template ribozyme consisting of ATRib's IGS−P1 closed by a tetraloop.

† This research was supported by NSF MCB-9982237 to H.S. A.F-C. acknowledges the Mark Diamond Research Fund for generous support.

* To whom correspondence should be addressed. E-mail: hsuga@acsu.buffalo.edu; phone: 716-645-6800, ext. 2170; fax: 716-645-6963.

[1] Abbreviations: ATRib, aminoacyl-transferase ribozyme; $ATRib^{TL}$, ATRib containing two tetraloop substitutions; $ATRib^{TLP}$, $ATRib^{TL}$ containing 31 additional nucleotides at the 3′-end; ATP, adenosine triphosphate; biotin-Met, *N*-biotinylated L-methionine; DEPC, diethyl pyrocarbonate; EDTA, ethylenediaminetetraacetic acid; IGS, internal guide sequence; MOPS, 3-[*N*-morpholino]propanesulfonic acid; PAGE, polyacrylamide gel electrophoresis; PCR, polymerase chain reaction; SAv, streptavidin.

10.1021/bi011102k CCC: $20.00
Published on Web 10/17/2001

activity (Figure 1A). Extensive metal-dependent kinetics on this tandem G:C mutant revealed that this mutation increased the dissociation constant for $Co(NH_3)_6^{3+}$ by 50-fold (*11*). These observations, along with the X-ray and NMR structural information for tandem G:U wobble pairs complexed with $Co(NH_3)_6^{3+}$ (*12*, *13*), lead us to hypothesize that the major groove of the tandem G:U pairs may constitute a metal binding site for a hexahydrated Mg^{2+} or $Co(NH_3)_6^{3+}$ ion, of which water or ammonium ligands coordinate to the oxyanion intermediate in the transition state of acyl-transfer reaction.

However, results obtained from the template ribozyme (Figure 1B) revealed that the presence of the tandem G:U pairs and the IGS alone is not sufficient for complete catalytic activity of ATRib (*8*). This implies that other structural elements in ATRib are directly involved in catalysis. Therefore, we have devoted our efforts to determine the essential catalytic and structural motifs and how these motifs participate in catalysis. Three methods were used in this study: phylogentic analysis of ATRib variants generated by in vitro evolution, extensive mutational analyses, and hydrolytic metal ion cleavage of ATRib and mutants in the presence of increasing concentrations of a competing catalytically active metal ion.

MATERIALS AND METHODS

In Vitro Selection of ATRib and Construction of Mutants. The selection was carried out by the same procedure as previously reported (*7*, *9*). The DNA templates for the mutants were constructed by PCR using the appropriate DNA primers containing mutations, similar to the procedures described elsewhere (*8*, *9*). For $ATRib^{TLP}$, the 3′-primer, 5′-*GCTCA ACGAA* <u>*GTAGG ACTTAC GATGT ACGTC C*</u>CAAC CAAAA ACAAA AAGCA TCACG TATGA T-3′, was used for PCR amplification of DNA template of $ATRib^{TL}$ to incorporate the complementary sequence of the italicized bases into $ATRib^{TL}$. Note that the underlined sequence was derived from the original 3′-primer used for the selection (*8*, *9*).

Kinetic Assays. General kinetic assays were performed as follows: A 1 μL solution of ca. 5 μM [^{32}P]-body-labeled ATRib or mutant in 5 μL of DEPC water and 1 μL of 10× MK buffer (250 mM MOPS, 1 M KCl at pH 7.0) was heated at 95 °C for 2 min and cooled to 25 °C over 5 min. To this solution was added 1 μL of 10× $MgCl_2$ (500 mM) and equilibrated for 5 min, to give a total of 8 μL of ribozyme solution. The reaction was initiated by the addition of 2 μL of 10 μM biotin-L-Met-3′-ACCAAC-5′ or 100 μM biotin-L-Met-3′-ACCA-5′, giving the final concentrations of ca. 0.5 μM ribozyme and 2 or 20 μM of substrate in 25 mM MOPS, 100 mM KCl, and 50 mM $MgCl_2$. A 1 μL aliquot was removed at various time points and quenched by the addition of 4 μL of MEUS buffer (25 mM MOPS, 5 mM EDTA, 8 M urea, and 10 mM SAv, pH 6.5). The products were analyzed by 8% PAGE at 4 °C and quantified using the Molecular Imager FX (Bio-Rad). Note that under these conditions all ribozymes were saturated with the substrate, so that the observed rate constant (k_{obs}) for each ribozyme should approximate its maximal value (k_{cat}). Velocities were determined by taking at least five points from the linear regions of the time course and fit using the KaleidaGraph graphing and curve fitting package (Abelbeck Software). The k_{obs} was derived from the average of rates from 2 to 3 kinetic experiments and corrected to the relative rate based on the k_{cat} of the wild-type ATRib.

Lead-Induced and Terbium-Induced Cleavage. The folded ca. 0.25 μM 5′-[^{32}P]-labeled $ATRib^{TLP}$ or mutant in MK buffer was incubated at room temperature with 100 μM $Pb(OAc)_2$ for 5 h, or 20 μM $TbCl_3$ for 2 h, in the presence of increasing concentrations of $MgCl_2$ or $Co(NH_3)_6^{3+}$. More details regarding the concentrations of the metal ions are presented in the figure legends. Reactions were quenched by the addition of EDTA to a final concentration of 75 mM, and ethanol precipitated. RNase T1 digestions were performed under conditions described in the literature with minor modifications (*14*). Samples were analyzed by 8% PAGE and were visualized and quantified using the Molecular Imager FX (Bio-Rad).

Inhibition and Stimulation of Catalysis by Monovalent Ions. Inhibition experiments were performed as described in the general kinetic assays, except that various concentrations of monovalent metal ion chloride solution in DEPC water replaced DEPC water to give the desired final concentrations as shown in Figure 9. In the case of Na^+ stimulation experiments, a final concentration of 10 mM of EDTA was added to remove traces of contaminating multivalent metal ions.

RESULTS AND DISCUSSION

New Classes of Acyl-Transferase Ribozymes Reveal Conserved Motifs. One convenient approach to identify the essential nucleotides within a catalytically active RNA molecule is through a phylogenetic comparison. Unfortunately, the original selection resulted in only one major class of ribozymes, which contained E18, the parent sequence of the engineered ATRib (*8*). To obtain additional sequence populations of acyl-transferase ribozymes, we returned to the 10th-round pool RNA and subjected it to increased selective pressures. Three rounds of stringent selection with decreased pH, Mg^{2+} concentration, and incubation time, yielded a new population of active RNAs with enhanced sequence diversity, as described elsewhere (*15*). These ribozymes were categorized into five independent classes (I−V) based on their primary sequence similarities. Preliminary metal-dependent kinetic studies revealed that both Mg^{2+} and $Co(NH_3)_6^{3+}$ could support catalysis of ribozymes in classes I−IV. On the other hand, class V, which includes the HS01 ribozyme, has a distinct metal dependency, i.e., it utilizes Mg^{2+} but not $Co(NH_3)_6^{3+}$ (*15*).

Although the primary sequences of classes I−III are dissimilar, ribozymes in these classes share some sequence features: a GAAA sequence and tandem Us adjacent to IGS. The secondary structure of a representative sequence of each class was predicted using the Zuker algorithm (*16*). All three independent classes of ribozymes fall into remarkably similar cloverleaf-type secondary structures (Figure 2) and display two characteristic motifs that are conserved in all three classes: (i) an internal guide sequence (IGS) and tandem G:U wobble base pairs in the P1 region and (ii) a GAAA-loop and a G:U wobble base pair in the P3 region. These common structural features allow us to hypothesize that these conserved motifs comprise the catalytic core of ATRib.

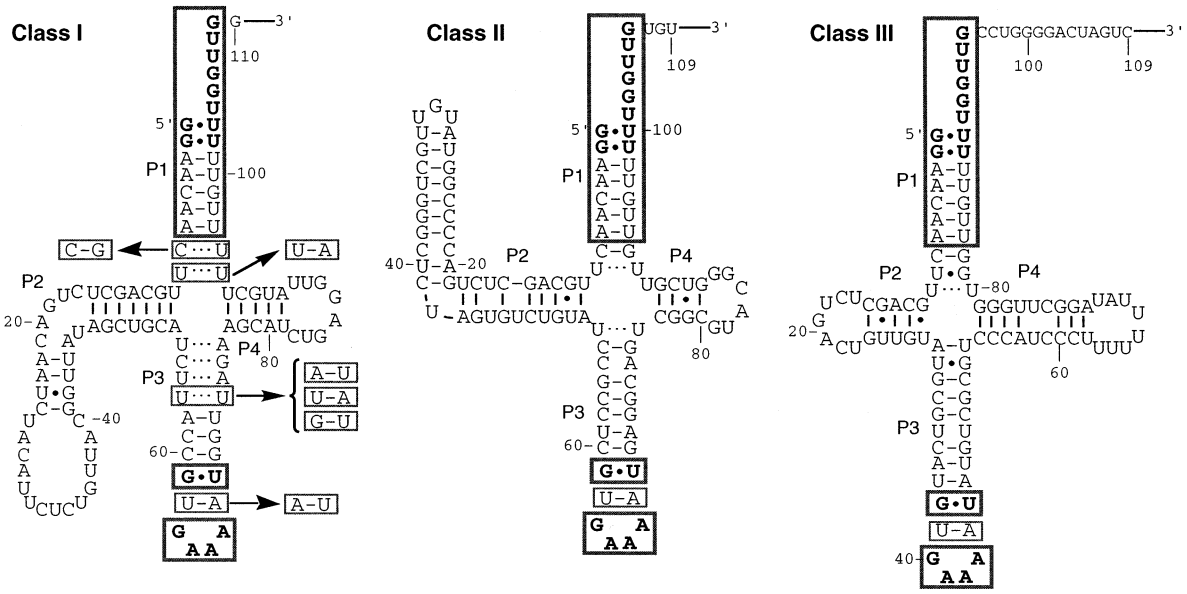

FIGURE 2: The secondary structure of representative clones in three classes of ATRib. The 3′-end 20-nt constant primer sequence is shown in a solid line. Sequences in bold boxes are conserved in class I−III ribozymes (*15*). Mutations of base pairs observed in ribozyme variants in each class are shown in the boxes.

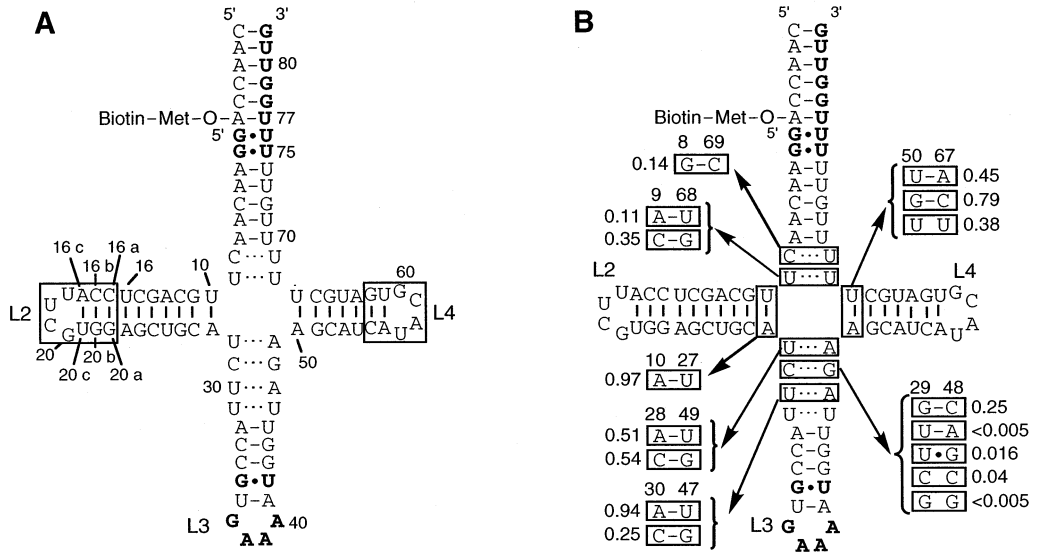

FIGURE 3: Mutational studies on ATRib^{TL}. (A) The secondary structure of ATRib^{TL} where hairpin stem-loops were introduced in L2 and L4. Newly introduced loops are highlighted in boxes. (B) Mutations introduced in joining regions. Mutations are highlighted in boxes, and the value for each mutant is relative to the catalytic rate of the wild-type ATRib (*8*).

L2 and L4 Can Be Replaced with Stable Tetraloops. The variations found in L2 and L4 of the class I−III ribozymes in the above phylogenetical analysis suggest that these loops do not participate in catalysis directly. To establish the lack of importance of L2 and L4 in the structure, an ATRib mutant was constructed in which these loops were substituted with stable stem-tetraloops (*17*, *18*) (Figure 3A). This ribozyme, referred to as ATRib^{TL}, exhibits a virtually identical initial rate as wild-type ATRib (*8*), providing strong evidence that the sequence of neither L2 nor L4 is critical for catalysis (data not shown). Despite the similar activities of ATRib^{TL} and ATRib, we found that the end point of self-aminoacylated ATRib^{TL} is slightly higher than that of ATRib (∼70 vs ∼50%). When the folded ribozymes were analyzed on native PAGE, ATRib^{TL} showed two distinct bands, in an approximate ratio of 2:8, whereas ATRib showed three distinct bands, in a ratio of 2:6:2 (D. Padalino and H. Suga, supporting data). Since we expect that the major band should correspond to the active fold of ATRib^{TL} and also the mobility of the minor band was the same as that of a band in the absence of K^+ ion, we assigned the major and minor bands to the folded and unfolded forms, respectively. The second minor band observed for ATRib is likely a misfolded structure. These results indicate that the incorporation of stable tetraloops into L2 and L4 increases the fraction of correctly folded ribozymes. Since structural mapping described below would be influenced by the populations of unfolded or misfolded structure, it is critical to use a better folder of ribozyme to minimize the background hydrolysis unrelated to the active folder. Hence, all further structural analyses of the ribozyme were pursued using ATRib^{TL}.

The Joining Region Governs the Tertiary Fold. Although in earlier papers the bases in the joining (J) region (boxed bases in Figure 3B) were shown to be unpaired (*8*, *9*), an

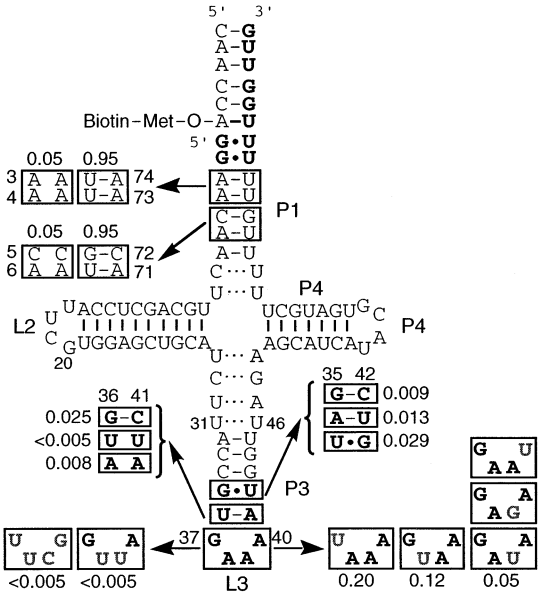

FIGURE 4: Mutational studies on ATRib^{TL} in the catalytic core. Mutations introduced in the catalytic core region are highlighted in boxes and resulting relative activities to the wild type (*8*) are reported.

extensive comparison of the variants in class I ATRib suggests that some of these bases participate in base pair interactions. To explore the J region base pairing, a total of 16 mutants based on ATRib^{TL} were prepared and tested for self-aminoacylation activity. In most cases, the compensatory mutants that preserved the base pairing exhibited nearly identical or slightly reduced activity (2−3-fold) when compared to wild type (Figure 3B). However, incorporation of inverted Watson−Crick (W−C) base pairs into certain positions, such as C29:G48, or introduction of W−C base pairs into the assumed noncanonical base pairs at C8:U69 and U9:U68 did not maintain appreciable catalytic activity. Presumably, these bases are preferred at these positions within the J region due to the hydrogen bonding networks that govern the proper tertiary folding of ATRib.

Conserved Motifs Play Critical Roles in Catalysis. Comparison of classes I−III of the ribozyme has led us to speculate that the catalytic core is comprised of the conserved regions of L3−P3 and IGS−P1. Previous work has suggested that the tandem G:U wobble base pairs (G1−G2/U75−U76) near the acylation site play critical roles in catalysis, presumably by forming the metal ion binding site (*11*). However, the catalytic roles of the remaining conserved residues in the P1 and L3−P3 regions remain unknown. In an effort to explore the importance of these conserved regions, we generated a series of mutants based on ATRib^{TL}.

Since the A3−A7 sequence in P1 was a part of the constant primer region for the selection, its complementary counter sequence, U70−U74, may have been selected due to W−C base pairing rather than a direct role in catalysis. To investigate this stem motif, we constructed mutants that contain single and double compensatory base pairs within this region. As expected, misparing in P1 was detrimental, whereas reforming the stem interactions by compensatory mutations rescued the wild-type activity (Figure 4). These observations affirm that the conserved sequence in P1, except for the tandem G:U wobble pairs, simply plays a role in forming the stem structure.

The GAAA loop in L3 is a completely conserved structural motif within classes I−III of the ATRib family. The GAAA loop is a member of the GNRA (N = any base, and R = G or A) loop family that occurs frequently in RNA molecules and has been characterized to be a stable tetraloop motif (*19*−*21*). In addition, it is often involved in long-range tertiary interactions providing stabilization of the tertiary structures (*22*−*27*). For instance, a GAAA loop in the P4−P6 domain of the *Tetrahymena* ribozyme interacts with its acceptor motif and plays critical roles in both structural stabilization and catalysis (*24*). We therefore hypothesize that the conserved L3 GAAA loop in the ATRib family may be involved in structural stabilization and/or catalysis.

The stability of the GAAA loop relies on the specific interactions between its four bases, such as hydrogen bonding between the first G and the third A, as well as stacking of three As (*19*−*21*). Therefore, mutations within the GAAA loop may disturb loop stability, which may in turn disrupt the critical tertiary structural interactions. We examined the replacement of the GAAA loop with another known stable tetraloop, UUCG (*28*). This mutation resulted in a greater than 200-fold decrease in activity, which was similar to that observed for the template ribozyme (Figure 1B). This result confirms that the L3 GAAA loop is a critical structural motif for the ATRib activity. To gain more insight into the necessity of the sequence, we introduced single or double base substitutions into the GAAA loop.

The results are summarized in Figure 4. Single U mutations in the tetraloop reduced activities by 5−20-fold. It should be noted that the G37U mutation, which disrupts the loop stability most significantly, exhibited the mildest reduction in activity of all the single-U-substitution mutants that were tested. This suggests that the GAAA loop is not simply acting as a stable loop but is likely playing a more specific role, possibly through an interaction(s) with other structural motifs. This view is further strengthened by the observations that (i) the A39G mutation that forms a GAGA loop (another member of GNRA loop family) results in a 20-fold reduction of activity and (ii) the double mutations of the GAAA to the GUUA loop reduced the catalytic activity to the level of the template ribozyme (Figure 1B). These mutational experiments explicitly demonstrate an essential role of the L3 GAAA loop in catalysis.

Another conserved motif is the G35:U42 wobble pair in the P3 stem. Mutation of this wobble pair to G:C, A:U, or U:G pairs reduced the activity by 50−100-fold, again suggesting its critical role in catalysis. When the primary sequences of variants found in class I−III were compared, the U36:A41 pair situated between the above two conserved motifs allowed only the substitution of the inverted pair, A36:U41 (Figure 2). We, therefore, explored the ability of this A:U pair to accommodate mutations, by testing mutants containing C:G, U:U, and A:A pairs at this position. Results of these mutations showed a larger than 40-fold reduction of activity (Figure 4), suggesting that an A:U pair, in either orientation, is required to close this tetraloop. The above results are consistent with the idea for the formation of G35:U42 and A36:U41 pairs, but this does not exclude that they may interact in some noncanonical fashion.

Thus, our mutational studies show that the conserved sequences play critical roles in catalysis. Questions that remain unanswered are how these motifs constitute the

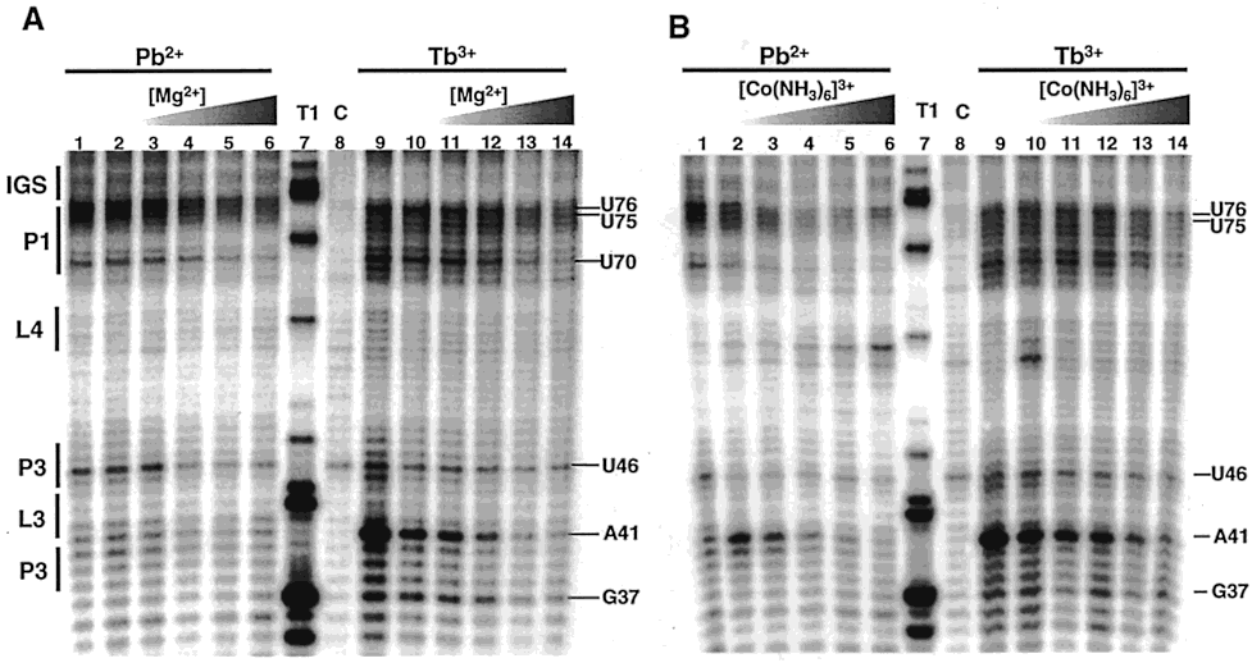

FIGURE 5: Pb^{2+}- and Tb^{3+}-induced cleavage analyses of $ATRib^{TLP}$. Unless otherwise noted, all assays were incubated at room temperature: Pb^{2+} incubation for 5 h and Tb^{3+} incubation for 2 h. The concentrations for Pb^{2+} and Tb^{3+} used are 100 and 20 μM, respectively (see also Materials and Methods). C (control) denotes no cleaving reagents (lane 8), and T1 denotes a limited digestion with RNases T1 (lanes 7). (A) Pb^{2+}- and Tb^{3+}-induced cleavage of $ATRib^{TLP}$ with increasing Mg^{2+} concentrations. Lanes are Pb^{2+} cleavage with Mg^{2+} concentrations of 0, 0.1, 0.25, 0.5, 1.5, and 10 mM (lanes 1−6), Tb^{3+} cleavage with Mg^{2+} concentrations of 0, 10, 15, 30, 50, and 100 mM (lanes 9−14). (B) Pb^{2+} (lanes 1−6) and Tb^{3+} (lanes 9−14) induced cleavage with increasing $Co(NH_3)_6^{3+}$ concentrations of 0, 0.1, 0.25, 0.5, 1, and 2 mM.

catalytic core, and what their specific roles are in catalysis. Since it has been proposed that the conserved tandem G:U wobble pairs in P1 play a role in forming a metal binding site, we decided to explore extensively the roles of these conserved sequences in the relation to the catalytic metal ion.

Pb^{2+} and Tb^{3+} Cleave the Conserved Regions Strongly. Lead (Pb^{2+}) and terbium (Tb^{3+}) ions have been used to identify both structurally relaxed or single stranded regions, such as loops and bulges (*29*−*33*), as well as high affinity metal ion binding sites in RNA molecules (*15*, *33*−*37*). It has been shown that these ions are able to bind to the same or similar sites as Mg^{2+} ions (*35*, *38*) and are therefore effective probes for detection of Mg^{2+} binding sites. To probe the high affinity metal binding sites in ATRib, we performed metal-dependent cleavage of a 5′-[^{32}P]-labeled $ATRib^{TL}$ derivative (vide infra) at low concentrations of Pb^{2+} and Tb^{3+}. It should be noted that at high concentrations of these hydrolytic metal ions cleavage was observed at the structurally accessible sites such as the L2&L4 and joining regions, along with some unexpected nonspecific sites. The nonspecific cleavage is presumably due to perturbations in the tertiary fold of $ATRib^{TL}$. We therefore performed all experiments described here at low concentrations of hydrolytic metal ions under carefully optimized conditions.

Since the 3′-end of $ATRib^{TL}$ is the hexanucleotide IGS, it is difficult to clearly monitor the cleavage profile at this site. To resolve this issue, we constructed an $ATRib^{TL}$ derivative, referred to as $ATRib^{TLP}$, which contains 31 additional nucleotides downstream of IGS (see Materials and Methods). This $ATRib^{TLP}$ showed an identical activity to the parental $ATRib^{TL}$ (data not shown), and therefore $ATRib^{TLP}$ and its mutants were used for most probing experiments described below. Note that the folding procedure for ATRib (the parental ribozyme of $ATRib^{TLP}$) is carried out in the MK buffer without Mg^{2+} (see Materials and Methods). The $ATRib^{TLP}$ were folded by the same method and therefore should yield the correctly folded tertiary structure.

The addition of low concentration of Pb^{2+} and Tb^{3+} to $ATRib^{TLP}$ in the absence of Mg^{2+} induced cleavage at nearly identical sites, A41 (P3), U46 (P3), U70 (P1), U75−U77 (P1), and the single-stranded region at the downstream of IGS (Figure 5A, lanes 1 and 9 for Pb^{2+} and Tb^{3+}, respectively). However, stronger intensities at certain cleavage sites were noted: In the case of Pb^{2+} substantial cleavage occurred at U75−U77, whereas in the case of Tb^{3+} a heavy cleavage at A41 was also observed along with those at U75−U76. The observed metal-species dependence of cleavage intensities can be attributed to the preferential binding of Pb^{2+} and Tb^{3+} toward U75−U77 and A41, respectively, due to their size and electrostatic strength. Most importantly, the addition of Mg^{2+} effectively competes with Tb^{3+} at these two sites, resulting in inhibition of the cleavage of both sites (Figure 5A, Tb^{3+} panel, lanes 10−14) with a nearly equal decaying profile. This simultaneous decrease in cleavage intensity is consistent with the hypothesis that these two sites constitute a single metal binding site. The experiments using $Co(NH_3)_6^{3+}$ as a competitor for Tb^{3+} also exhibited similar decaying profiles at the same cleavage sites (Figure 5B, Tb^{3+} panel, lanes 10−14). The only notable difference between $Co(NH_3)_6^{3+}$ and Mg^{2+} is that lower concentrations of $Co(NH_3)_6^{3+}$ are required to yield the same decaying profiles, which is consistent with previous kinetic results where $Co(NH_3)_6^{3+}$ has a significantly lower K_d for ATRib than Mg^{2+} (0.35 vs 14 mM) (*11*). On the basis of the above cleavage results, we propose that the A41 and U75−U76 regions are the

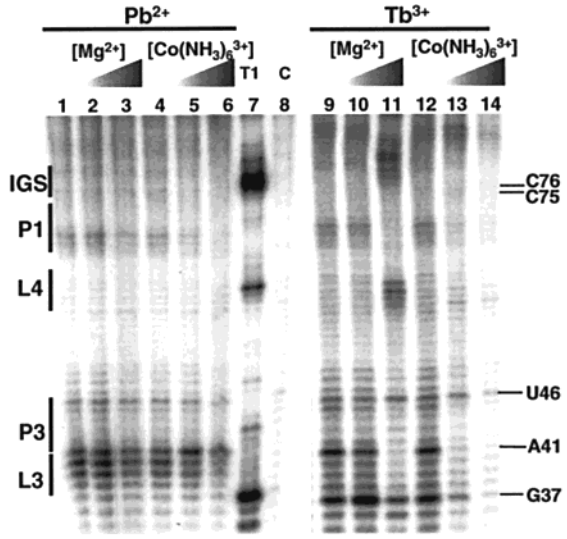

FIGURE 6: Pb^{2+} (lanes 1−6) and Tb^{3+} (lanes 9−14) induced cleavage of the U75C/U76C mutant of $ATRib^{TLP}$. The concentrations for Pb^{2+} and Tb^{3+} used are 100 and 20 μM, respectively (see also Materials and Methods). The concentrations of Mg^{2+} are 0, 0.75, 12.5 mM (lanes 1−3) and 0, 10, 100 mM (lanes 9−11), the concentrations of $Co(NH_3)_6^{3+}$ are 0, 0.1, 0.5 mM (lanes 4−6) and 0, 8, 50 mM (lanes 12−14). C (control) denotes no cleaving reagents (lanes 8 and 15), and T1 denotes a limited digestion with RNase T1 (lanes 7 and 16). It should be noted that the cleavage profile similar to lane 11 has been consistently observed when an excess $Co(NH_3)_6^{3+}$ or Mg^{2+} was added in solution (data not shown). In this case, the cleavage sites are in structurally accessible region such as L4 and the unstructured region adjacent to IGS.

potential high affinity metal binding motifs for Mg^{2+} and $Co(NH_3)_6^{3+}$.

It should be noted that the Hill analysis of the rate constant as a function of concentration of Mg^{2+} or $Co(NH_3)_6^{3+}$, in the presence of spermidine, indicate the involvement of a single specific metal ion (*11*). In light of these observations, we can extrapolate that both cleavage sites competed by Mg^{2+} and $Co(NH_3)_6^{3+}$ constitute a single binding site in the tertiary space. The tandem G:U wobble pairs, G1−G2/U75−U76, is the proposed catalytic metal binding site, and the explicit cleavage at U75−U76 by both hydrolytic metal ions provides additional support for this idea. We, therefore, propose that the above two high affinity metal binding motifs constitute a single concerted metal binding site.

Pb^{2+} and Tb^{3+} Cleave $ATRib^{TLP}$ Mutants Differently from the Wild Type. We have shown that mutations of the conserved catalytic motifs, including the above metal binding sites (Figure 4), are detrimental for catalytic activity. The double mutation of U75−U76 to C75−C76 (U75C−U76C) is known to reduce the catalytic activity potentially due to the disruption of the metal binding site. To further verify our hypothesis for the concerted metal binding site, we explored Pb^{2+} and Tb^{3+} cleavage of this double mutant of $ATRib^{TLP}$ (Figure 6). Pb^{2+} and Tb^{3+} cleavage profiles of this mutant did not show cleavage sites at unexpected regions such as stems, indicating that the overall tertiary structure of this mutant was maintained in the presence of these hydrolytic metal ions (Figure 6). The cleavage at the C75−C76 region, for which strong cleavage was observed in the wild type, was completely wiped out in both Pb^{2+} and Tb^{3+} cleavage experiments. It should be noted that the intense Tb^{3+} cleavage at A41 observed for the wild type significantly decreased in this mutant, and instead G37 was strongly cleaved (lanes 9 and 12). The addition of Mg^{2+} and $Co(NH_3)_6^{3+}$ inhibited the Tb^{3+} cleavage at both A41 and G37 (lanes 10 and 11 and lanes 13 and 14). Interestingly, NMR analyses of GAAA-stem loop motifs complexed with $Co(NH_3)_6^{3+}$ have shown that $Co(NH_3)_6^{3+}$ localizes between the first G and the second and third As of the loop (*39*−*41*). The intense cleavage at G37 in the U75C−U76C mutant suggests that the disruption of the concerted metal binding site results in the localization of Tb^{3+} to the general metal binding site at G37 within the GAAA loop, as opposed to the highly specific binding site at A41 in the wild-type $ATRib^{TL}$.

Thus, the mutation of the tandem G:U wobble pairs to the tandem G:C pairs simultaneously altered the cleavage profiles in both A41 and U75−U76 regions, suggesting that this approach might be effective for monitoring mutational disruptions of the concerted high affinity metal binding sites. With general considerations for this type of mutational experiments, it cannot be ruled out that the mutation(s) introduced to the wild-type ribozyme perturbed critical tertiary contacts unrelated to the metal binding site, thereby indirectly disturbing Pb^{2+} and Tb^{3+} cleavage sites. However, in the light of our previous observation that mutating U75C−U76C reduces catalytic activity and increases the dissociation constant of $Co(NH_3)_6^{3+}$ (*11*), we are fairly confident that the U75−U76 region closely relates to the metal binding site. Furthermore, since the U75C−U76C mutation still maintains the essential base pairs with G1−G2, the majority of the tertiary structure is very likely to remain intact except for the catalytic core. Thus, we believe that the observed change in the cleavage profiles of both A41 and U75−U76 by mutating U75C−U76C disrupts the catalytic core by affecting the concerted metal binding site. It should be noted that one important take-home message of the above experiment is that the choice of reagent is also critical to observe the disruption of the metal binding site, i.e., Pb^{2+} is more suitable for probing the U75−U76 region, while Tb^{3+} is more suitable for the A41 region, in our case.

The intense Tb^{3+}-induced cleavage and subsequent protection by Mg^{2+} and $Co(NH_3)_6^{3+}$ at position A41 led us to examine the effect of mutations of the bases surrounding A41 on hydrolytic cleavage. A mutant containing U36G:A41C, that displays a 40-fold reduction of the wild-type activity (Figure 4), was subjected to Pb^{2+} and Tb^{3+} cleavage. When compared to wild type (Figure 7A, all panels), this mutant showed a similar cleavage pattern throughout, with similar Pb^{2+} cleavage intensities in the P1 region (Figure 7B, panel 1, lanes 1−3), but with slightly decreased intensities for both Pb^{2+} and Tb^{3+} cleavage at position 41 (Figure 7B, panels 2 and 3, lanes 1−3). The similar cleavage pattern observed for this mutant suggests that the Mg^{2+} binding site is relatively independent of the actual nucleobase at position 41. These observations, coupled with the observation that the inverted U:A pair mutant retains activity, led us to speculate that this A:U pair does not directly participate in forming the metal binding site, but rather plays a structural role in maintaining an optimum tertiary interaction of the L3 GAAA loop with its counter motif (vide infra).

The G35:U42 wobble base pair in P3 was absolutely conserved in classes I−III, and the mutation of this pair to either U35:G42 or G35:C42 was detrimental for activity

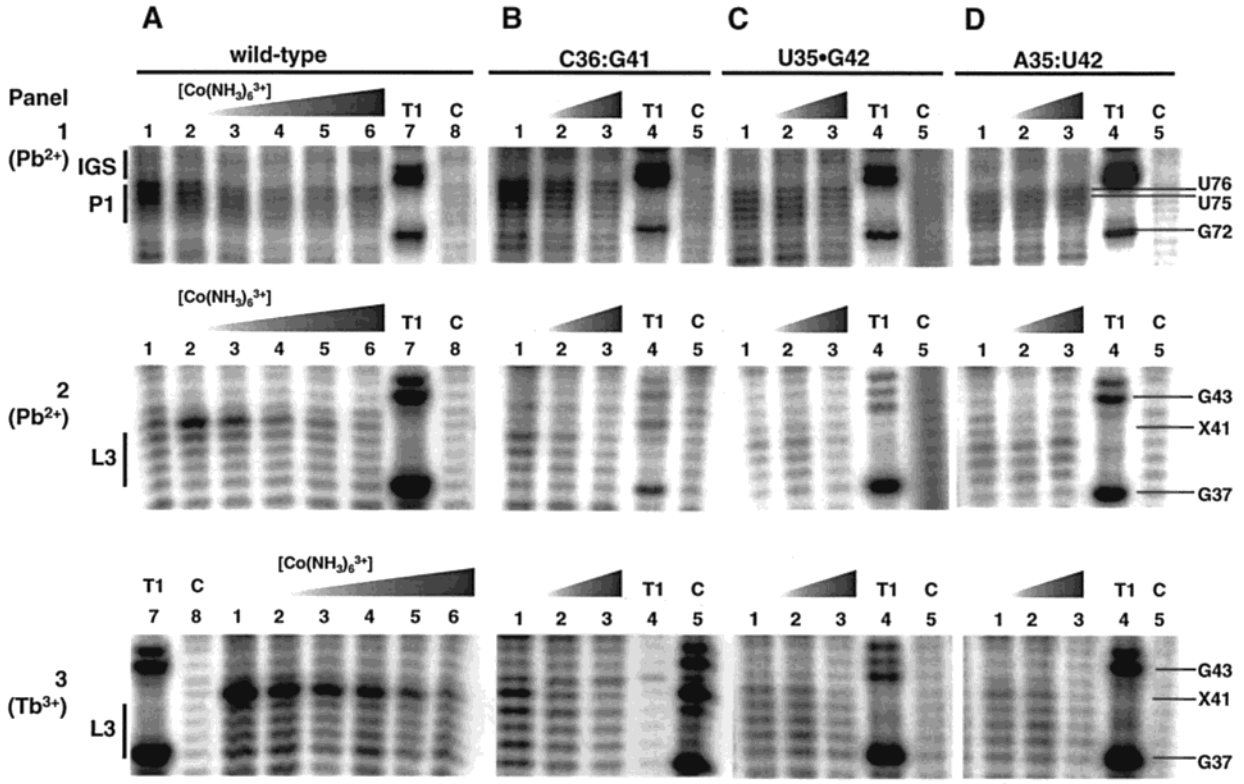

FIGURE 7: Pb^{2+}- and Tb^{3+}-induced cleavage analyses of wild-type $ATRib^{TLP}$ (A) and mutants C36:41G (B), U35:42G (C), and A35:42U (D). All cleavage assays of these mutants were performed with increasing $Co(NH_3)_6^{3+}$ concentrations. Panels 1 and 2 are the areas of interest for Pb^{2+} cleavage in P1 and P3−L3, respectively, and panel 3 is that for Tb^{3+} cleavage in P3−L3. (A) Pb^{2+} and Tb^{3+} cleavage of wild-type $ATRib^{TLP}$ with increasing $Co(NH_3)_6^{3+}$ concentrations of 0, 0.1, 0.25, 0.5, 1, and 2.5 mM (lanes 1−6 in all panels). (B) C36:41G mutant with increasing $Co(NH_3)_6^{3+}$ concentrations of 0, 0.25, and 2 mM (lanes 1−3 in all panels). (C) U35:42G mutant with increasing $Co(NH_3)_6^{3+}$ concentrations of 0, 0.3, and 2.5 mM (lanes 1−3 in all panels). (D) A35:42U mutant with increasing $Co(NH_3)_6^{3+}$ concentrations of 0, 0.25, and 2 mM (lanes 1−3 in all panels). C (control) denotes no cleaving reagents, and T1 denotes a limited digestion with RNases T1.

(Figure 4). The Pb^{2+} and Tb^{3+} hydrolyses of these two mutants displayed cleavage profiles, which differ from those of wild type (Figure 7C,D). The Pb^{2+} cleavages at U75−U76 in the absence of $Co(NH_3)_6^{3+}$ were weaker in the mutants than in the wild type, and the addition of $Co(NH_3)_6^{3+}$ did not show significant inhibition of the cleavage (panel 1). Moreover, the intense Tb^{3+} cleavage at A41 was completely diminished (panel 3). These observations strongly suggest that the G35:U42 wobble base pair is essential for the formation of the concerted metal binding site. We propose that the G35:U42 pair has two important aspects: The wobble configuration brings about (i) a distortion of phosphate backbone, which presumably makes the bridging phosphate between A41 and U42 more accessible to a metal ion for binding (an consequently cleavage by Pb^{2+} and Tb^{3+}) and (ii) an increase in negative electrostatic potential on the major groove surface (*12*). This wobble base pair and the A41−U42 bridging phosphate probably create a pocket that preferentially recruits a hexahydrated Mg^{2+} or $Co(NH_3)_6^{3+}$ in concert with the tandem G:U wobble base pair near the acylation site.

Tb^{3+} cleavage was also examined with two additional mutants, one that contains L3 UUCG loop and the other that lacks IGS (ΔIGS). In both mutants, the intense cleavage at A41 was retained with nearly identical intensity to the wild type (data not shown). The P1 region in the L3 UUCG mutant was also cleaved with a similar degree as the wild type (note that the cleavage of this region in the ΔIGS mutant could not be resolved due to the technical limitation for the resolution on PAGE). These results suggest that the necessity of the GAAA loop for activity is unrelated to the formation of the concerted metal binding site. Recall that mutational studies of the GAAA loop implicate it in playing a critical role in catalysis (Figure 4). The formation of the concerted Mg^{2+} binding site consisting of A41−U42 and the tandem G:U wobble pairs would position the P1 an P3 helices in a parallel manner, which potentially brings about the long-range tertiary interaction between the IGS and GAAA loop motifs (Figure 8A). We therefore propose that this long-range tertiary contact contributes to the rate acceleration of acyl-transfer and is independent for the interactions with the catalytic metal ion.

Double Compensatory Extensions of P1 and P3 Preserve the Activity. The above model, where the P1 and P3 stems are juxtaposed in a parallel manner, predicts that inserting base pairs into either the P1 or P3 stem should disrupt the formation of the catalytic core (Figure 8A). On the other hand, simultaneous extension of both stems may restore the interaction, and result in an active catalyst. One drawback of this approach is that the complete recovery of catalytic activity may be difficult because extension of the stem also introduces a helical twist that would affect the precise interaction of the catalytic residues. However, if activity is recovered by the P1−P3 double compensatory extensions as compared with the single extension in either stem, it is a good evidence for the parallel positioning of P1 and P3 in

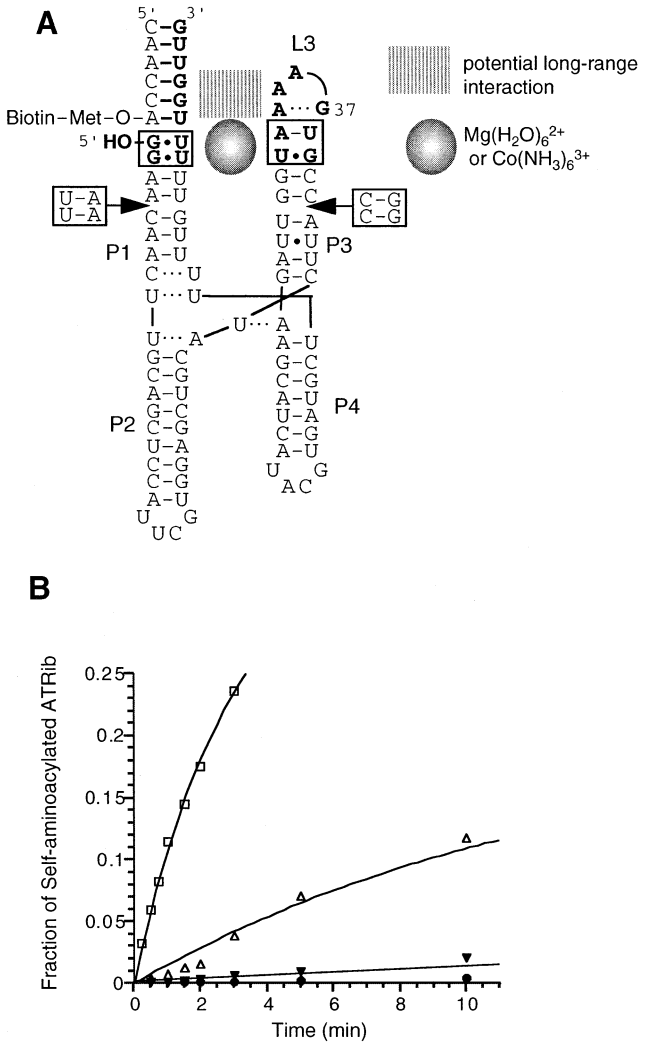

FIGURE 8: Schematic presentation of 3D model (A) and catalytic rates observed in mutants with extended P1 and P3 stems (B). (A) The catalytic core motifs are highlighted in boxes, and the bridging lines between these motifs indicate the proposed long-range interaction. A magnesium ion bound in the potential metal binding site is indicated by a gray sphere. The inserted base pairs in mutants are shown in boxes. Although P2 and P4 are shown in parallel, this orientation in the tertiary space has not been determined. (B) Fraction aminoacylated as a function of time for $ATRib^{TL}$ and mutants containing the insertion of two-base pairs in P1 and P3 stems. Wild-type $ATRib^{TL}$ (□), mutant with the double insertion into P1 and P3 (△), and mutants with the single insertion into P1 (▼) or P3 (●).

the ATRib tertiary structure. We prepared three mutants containing single and double two-base-pair insertions in P1 and P3 (Figure 8A). As expected, a single two-base-pair insertion into either P1 or P3 decreased the activity by more than 100-fold, whereas the simultaneous double two-base-pair insertions into both stems rescued activity, showing only an 8-fold reduction of the wild-type activity (Figure 8B). This result clearly supports our structural model of ATRib in which the P1 and P3 stems are juxtaposed in a parallel fashion, bringing about the long-range tertiary interaction that comprises the concerted Mg^{2+} binding site.

Monovalent Metal Ions Inhibit Mg^{2+}-Supported Activity at Low Concentrations, but Stimulate Activity at High Concentrations. The activity of ribozymes is most commonly dependent on the presence of divalent metal ions (*42*, *43*), although it has been shown recently that monovalent ions

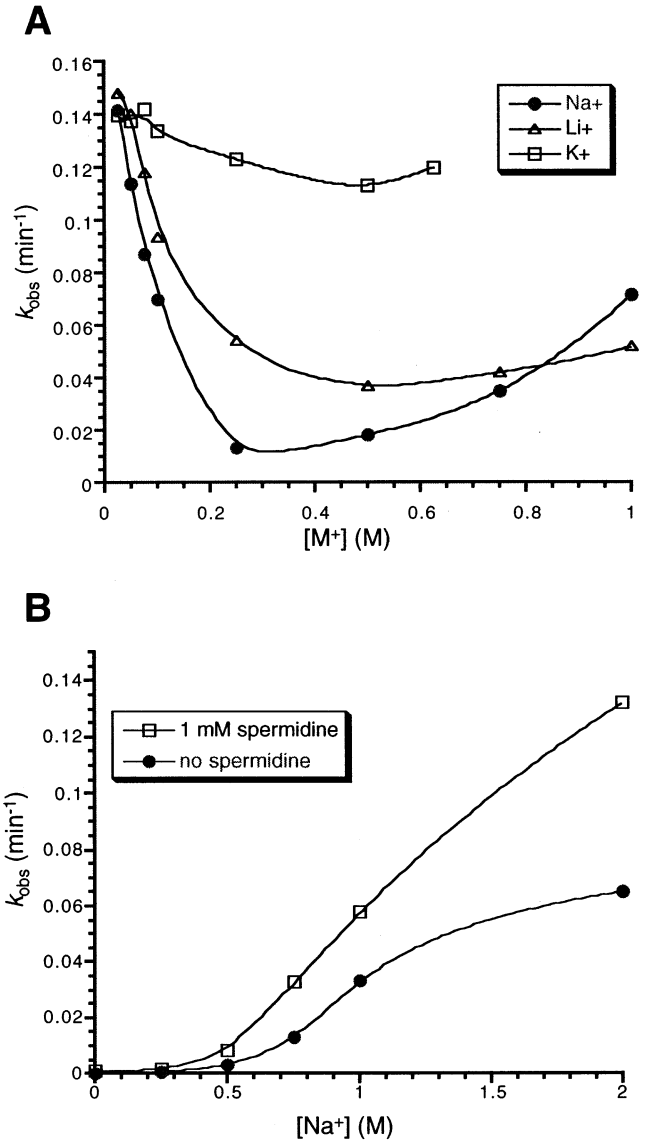

FIGURE 9: Monovalent ion-dependent inhibition and catalysis. (A) Inhibition and stimulation of Mg^{2+} supported catalysis by the presence of monovalent ions. Reactions were carried out in the presence of 10 mM $MgCl_2$, 25 mM MOPS adjusted by KOH, and various concentrations of monovalent ion. Data for K^+ (□), Li^+ (△), Na^+ (●) were fit to smooth interpolations. (B) Na^+ supported catalysis. Data for the presence (□) and absence (●) of spermidine were fit to smooth interpolations.

can also support catalysis (*44*−*46*). Exploration of the role of monovalent ions is of interest to further understand the mechanistic role of the catalytic metal ion in ATRib. Although potassium ions (K^+) were included in the selection buffer for the ATRib family, lowering the concentration of K^+ from 500 to 100 mM did not influence the catalytic activity, suggesting that K^+ is not an essential component for catalysis. To explore the monovalent ion dependence of ATRib in more detail, we determined the observed catalytic rate constant (k_{obs}) in the presence of 10 mM Mg^{2+} with various concentrations of monovalent ions (Figure 9A). As expected, the concentration of K^+ has very little effect on k_{obs}. In contrast, both Na^+ and Li^+ showed inhibitory behaviors. Na^+ is a very potent inhibitor, giving a K_i value of approximately 100 mM when 10 mM Mg^{2+} is present. This suggests that Na^+ can easily compete with Mg^{2+} for the Mg^{2+} binding site, yet is unable to promote catalysis.

Interestingly, at very higher concentrations of Na^+ (and Li^+) ribozyme activity recovers slightly. To determine whether this phenomenon is dependent on the monovalent ion alone, or a cooperative effect with Mg^{2+}, a titration of Na^+ in the absence of Mg^{2+} was performed (Figure 9B). Excess Na^+ appeared to be capable of supporting ribozyme catalysis, indicating that the increase of activity is Na^+-dependent. The addition of 1 mM spermidine also enhances the Na^+-supported activity by approximately 2-fold. The k_{obs} at 2 M Na^+ in the presence of 1 mM spermidine (Figure 9B) is similar to the value observed at 10 mM Mg^{2+} (Figure 9A), which is approximately 10-fold lower than k_{obs} ($= 1.3\ min^{-1}$) at saturating Mg^{2+} conditions (at 50 mM Mg^{2+} in the presence of 1 mM spermidine) (*11*).

The potent inhibitory activity observed for Na^+ can be attributed to the same hexahydrate coordination number and the similar size of Na^+ (1.02 Å) to that of Mg^{2+} (0.72 Å) (*35*). The replacement of Mg^{2+} with Na^+ in the metal binding site inhibits catalysis strongly, which implies that the charge of Mg^{2+} plays a critical role in catalysis. Why is the strong charge of metal ion important? It is clear that a metal ion that has a strong charge should bind the ribozyme strongly. However, if the strong charge is necessary for only binding, the addition of Na^+ should show cooperative enhancement of catalysis rather than the inhibition observed at low concentrations of Na^+. In light of observations for the X-ray structure of $Co(NH_3)_6^{3+}$-tandem G:U wobble pairs in P5b of group I intron (*12*) that is an analogous system to ours, the ligands of $Mg(H_2O)_6^{2+}$ or $Co(NH_3)_6^{3+}$ bound to the sites in ATRib can be located in a close position to the oxyanion of the aminoacyl-intermediate (*11*), and such a highly anionic species should be neutralized by an available cationic residue, which is most likely by metal cation. Therefore, the strong charge of metal ion is likely important for chemistry, in which the metal ion plays a role in effectively stabilizing the transition state of acyl-transfer reaction. Then, why do high concentrations of Na^+ support catalysis? This can be explained by a speculation that the role of metal ions is partially structural. It is possible that the presence of excess Na^+ may shield unfavorable repulsion between two helices of P1 and P3 and support the long-range interaction of the L3 GAAA loop with IGS that is also important for catalysis, resulting in the modest rate acceleration. The strong affinity of Mg^{2+} and $Co(NH_3)_6^{3+}$ to the metal binding site can bring about this tertiary interaction more effectively than Na^+. We thus conclude that the metal ion bound to ATRib plays both chemical and structural roles. Although this is our most favorable model for the metal ion roles in ATRib, it is still possible that Mg^{2+} and $Co(NH_3)_6^{3+}$ can play a purely structural role, where the metal ion exclusively interacts with the catalytic residues in the P1−P3 and IGS−L3 regions without any involvement of the metal ligands to interact with the oxyanion of the aminoacyl-intermediate.

CONCLUSION

On the basis of a phylogenetic analysis of the ATRib family in combination with mutational studies, we have revealed that the regions of P3−L3 and P1−IGS are the essential catalytic residues. Combined Pb^{2+} and Tb^{3+} hydrolytic cleavage assays on ATRib and mutants have successfully identified a concerted Mg^{2+} ion binding site. Specifically, the 35G:U42 wobble base pair and the U42-A41 bridging phosphate in P3, in concert with the electrostatic potential surfaces formed in the major groove of tandem G:U wobble base pairs in P1, create a specific and optimal site for $Mg(H_2O)_6^{2+}$ binding. We have shown that this single, fully hydrated catalytic metal ion can play both structural and chemical roles. We propose that water ligands bound to Mg^{2+} interact with the developing oxyanion intermediate, thereby stabilizing the transition state. We also speculate that the binding of Mg^{2+} to the catalytic site brings about the long-range tertiary interaction between the L3 GAAA loop and IGS. Together, these interactions orchestrate the rate acceleration seen for this ribozyme-catalyzed aminoacyl-transfer reaction.

ACKNOWLEDGMENT

We thank Anand Vaidya and David Hodgson for critical proof-reading and all members of the Suga group for helpful discussions. We also thank to Shinichi Watanabe for helpful discussions to build a 3D model of ribozyme.

SUPPORTING INFORMATION AVAILABLE

Native PAGE of ATRib and $ATRib^{TL}$ samples in various concentrations of K^+ (Supplementary Figure 1). This material is available free of charge via the Internet at http://pubs.acs.org.

REFERENCES

1. Cech, T. R., Zaug, A. J., and Grabowski, P. J. (1981) *Cell 27*, 487−496.
2. Guerrier-Takeda, C., Gardiner, K., Marsh, T., Pace, N., and Altman, S. (1983) *Cell 35*, 849−857.
3. Cech, T. R. (1990) *Annu. Rev. Biochem. 59*, 543−568.
4. Gold, L., Polisky, B., Uhlenbeck, O. C., and Yarus, M. (1995) *Annu. Rev. Biochem. 64*, 763−797.
5. Hager, A. J., Pollard, J. D., and Szostak, J. W. (1996) *Chem. Biol. 3*, 717−725.
6. Wilson, D., and Szostak, J. W. (1999) *Annu. Rev. Biochem. 68*, 611−647.
7. Lohse, P. A., and Szostak, J. W. (1996) *Nature 381*, 442−444.
8. Suga, H., Lohse, P. A., and Szostak, J. W. (1998) *J. Am. Chem. Soc. 120*, 1151−1156.
9. Lee, N., Bessho, Y., Wei, K., Szostak, J. W., and Suga, H. (2000) *Nat. Struct. Biol. 7*, 28−33.
10. Schimmel, P., and Kelley, S. O. (2000) *Nat. Struct. Biol. 7*, 5−7.
11. Suga, H., Cowan, J. A., and Szostak, J. W. (1998) *Biochemistry 37*, 10118−10125.
12. Cate, J. H., and Doudna, J. A. (1996) *Structure 4*, 1221−1229.
13. Kieft, J. S., and Tinoco, I. J. (1997) *Structure 5*, 713−721.
14. Toa, J., and Frankel, A. D. (1996) *Biochemistry 35*, 2229−2238.
15. Vaidya, A., and Suga, H. (2001) *Biochemistry*, *40*, 7200−7210.
16. Mathews, D. H., Sabina, J., Zuker, M., and Turner, D. H. (1999) *J. Mol. Biol. 288*, 911−940.
17. Molonaro, M., and Tinoco, I. (1995) *Nucleic Acids Res. 23*, 3056−3063.
18. Groebe, D. R., and Uhlenbeck, O. C. (1988) *Nucleic Acids Res. 16*, 11725−11735.
19. Tuerk, C., et al. (1988) *Proc. Natl. Acad. Sci. U.S.A. 85*, 1364−1368.
20. Heus, H. A., and Pardi, A. (1991) *Science 253*, 191−194.
21. SantaLucia, J., Kietzek, R., and Turner, D. H. (1992) *Science 256*, 217−219.

22. Pley, H. W., Flaherty, K. M., and McKay, D. B. (1994) *Nature 372*, 111−113.
23. Jaeger, L., Michel, F., and Westhof, E. (1994) *J. Mol. Biol. 236*, 1271−1276.
24. Murphy, F. L., and Cech, T. R. (1994) *J. Mol. Biol. 236*, 49−63.
25. Costa, M., and Michel, F. (1995) *EMBO J. 14*, 1276−1285.
26. Cate, J. H., Gooding, A. R., Podell, E., Zhou, K., Golden, B. L., Kundrot, C. E., Cech, T. R., and Doudna, J. A. (1996) *Science 273*, 1678−1685.
27. Abramovitz, D. L., and Pyle, A. M. (1997) *J. Mol. Biol. 266*, 493−506.
28. Cheong, C., Varani, G., and Tinoco, I. (1990) *Nature 346*, 680−682.
29. Kryzosiak, W. J. (1988) *Biochemistry 27*, 5771−5777.
30. Steicher, B., Ashen, U., and Schroeder, R. (1993) *Nucleic Acids Res. 21*, 311−317.
31. Ciesiolka, J., Hardt, W.-D., Schlegl, J., Erdmann, V. A., and Hartmann, R. K. (1994) *Eur. J. Biochem. 219*, 49−56.
32. Winter, D., Polacek, N., Halama, I., Streicher, B., and Barta, A. (1997) *Nucleic Acids Res. 25*, 1917−1824.
33. Hargittia, M. R., and Musier-Forsyth, K. (2000) *RNA 6*, 1672−1680.
34. Feig, A. L., Scot, W. G., and Uhlenbeck, O. C. (1998) *Science 279*, 81−84.
35. Feig, A. L., and Uhlenbeck, O. C. (1999) in *The RNA World* (Gesteland, R. F., Atkins, J. F., Eds.) pp 287−319, Cold Spring Harbor Laboratory Press, Cold Spring Harbor, NY.
36. Walter, N. G., Yang, N., and Burke, J. M. (2000) *J. Mol. Biol. 298*, 539−555.
37. Sigel, R. K., Vaidya, A., and Pyle, A. M. (2000) *Nat. Struct. Biol. 7*, 1111−1116.
38. Scott, W. G., Murray, J. B., Arnold, J. R. P., Stoddadr, B. L., and Klug, A. (1996) *Science 274*, 2065−2069.
39. Kuo, T.-C., and Herrin, D. L. (2000) *Nucleic Acids Res. 28*, 4197−4206.
40. Rudisser, S., and Tinoco, I., Jr. (2000) *J. Mol. Biol. 295*, 1211−1223.
41. Maderia, M., Horton, T. E., and DeRose, V. J. (2000) *Biochemistry 39*, 8193−8200.
42. Steitz, T. A., and Steitz, J. A. (1993) *Proc. Natl. Acad. Sci. U.S.A. 90*, 6498−6502.
43. Pyle, A. M. (1993) *Science 261*, 709−714.
44. Murray, J. B., Seyhan, A. A., Walter, N. G., Burke, J. M., and Scott, W. G. (1998) *Chem. Biol. 5*, 587−595.
45. O'Rear, J. L., Wang, S., Feig, A. L., Beigelman, L., Uhlenbeck, O. C., and Herschlag, D. (2001) *RNA 7*, 537−545.
46. Curtis, E. A., and Bartel, D. P. (2001) *RNA 7*, 546−552.

BI011102K